
Neural Proposals, Symbolic Guarantees: Neuro-Symbolic Graph Generation with Hard Constraints

Chuqin Geng^{1,2} Li Zhang² Mark Zhang² Haolin Ye¹ Ziyu Zhao¹ Xujie Si²

Abstract

We challenge black-box purely deep neural approaches for molecules and graph generation, which are limited in controllability and lack formal guarantees. We introduce Neuro-Symbolic Graph Generative Modeling (NSGGM), a neurosymbolic framework that reapproaches molecule generation as a scaffold and interaction learning task with symbolic assembly. An autoregressive neural model proposes scaffolds and refines interaction signals, and a CPU-efficient SMT solver constructs full graphs while enforcing chemical validity, structural rules, and user-specific constraints, yielding molecules that are correct by construction and interpretable control that pure neural methods cannot provide. NSGGM delivers strong performance on both *unconstrained generation* and *constrained generation* tasks, demonstrating that neuro-symbolic modeling can match state-of-the-art generative performance while offering explicit controllability and guarantees. To evaluate more nuanced controllability, we also introduce a *Logical-Constraint Molecular Benchmark*, designed to test strict hard-rule satisfaction in workflows that require explicit, interpretable specifications together with verifiable compliance.

1. Introduction

Generative modeling of graph-structured data is a fundamental challenge with profound implications for scientific discovery and engineering (Brockschmidt et al., 2019). From designing novel molecules and materials (Liu et al., 2018a; Cao & Kipf, 2018) to discovering electronic circuits (Chang et al., 2024), the ability to generate controllable graphs is a

key tool for innovation. However, molecular graph generation remains challenging due to the non-sequential nature of graphs, combinatorial sparsity, and the need to preserve chemical and guidance control.

These difficulties have motivated many generative models. Despite their success, deep molecular generative models (i.e. VAEs, autoregressive models, flows, diffusion) enable the exploration of the chemical space and are commonly evaluated using standardized distributional and diversity metrics (Brown et al., 2019) (Polykovskiy et al., 2020). However, as structural constraints are typically learned implicitly rather than specified as explicit rules, these methods generally do not provide formal certificates for user-specified constraints. Additionally, unless constraint compliance is learned during training or enforced during generation, hard user-specified constraints are often handled via post-hoc filtering, which does not scale with increased scaffold size (Maziarz et al., 2022). In high-stakes domains where transparency and interpretability is critical (Amann et al., 2020), this motivates methods that allow users to state hard constraints explicitly and verify satisfaction with checkable certificates, rather than relying on implicit neural control.

Motivated by these limitations, we introduce **Neuro-Symbolic Graph Generative Modeling (NSGGM)**, a neural-symbolic framework reframing molecule generation as a dual problem of scaffold and interaction learning and symbolic constraint modeling task. Our approach begins by decomposing molecules into a vocabulary of motifs/fragments (subgraph tokens) equipped with *interface information* and *neural guidance* specifying how they may connect to neighboring motifs, while deriving a set of symbolic assembly constraints over these interfaces. Benefiting from symbolic assembly, the neural component can focus on learning data-driven prior and providing high-level guidance, while an SMT solver (Barrett & Tinelli, 2018) enforces hard structural rules, guarantees constraint satisfaction by construction, and provide a transparent, verifiable layer of which constraints are satisfied.

While we share the idea of assembling predefined substructures with fragmented-based generative models (Jin et al., 2018; Mercado et al., 2021; Jin et al., 2020b), the key distinction is how assembly is performed. Prior methods typically

*Equal contribution ¹ School of Computer Science, McGill University, Montreal, Canada ² Department of Computer Science, University of Toronto, Toronto, Canada . Correspondence to: Chuqin Geng <chuqin.geng@mail.mcgill.ca>, Li Zhang <lizhang@cs.toronto.edu>, Xujie Si <six@cs.toronto.edu>.

approach assembly with a neural component entirely, where constraint sanctification is handled implicitly with any additional requirements being enforced via conditioning or post-hoc checks / rules rather than explicit, verifiable rules. To contrast, NSGGM takes a neuro-symbolic approach by separating learned-high level proposal from exact assembly under explicit constraints, allowing for transparent and certifiable sanctification of hard requirements. In summary, our key contributions are:

- We propose a two-stage neuro-symbolic pipeline where a lightweight neural model proposes subgraph tokens and provides global attachment / local interaction influence, and a symbolic SMT solver assembles a final graph by enforcing hard constraints by construction.
- NSGGM offers transparency, user-steerable controllability via explicit user-definable constraints expressed in the symbolic layer, while allowing the neural layer to complete unconstrained regions; this supports two complementary modes: (i) conditioning-based completion from user-supplied scaffolds, and (ii) constraint-driven synthesis subject to specified structural or topological constraints.
- We demonstrate that NSGGM achieves strong performance on unconstrained generation benchmarks and scaffold-conditioned generation, and present a case study of hard logical constraints with quantitative evaluation that highlights explicit constraint satisfaction and the transparency enabled by symbolic specifications.

2. Preliminaries

2.1. Graph Generation Tasks

The primary goal of graph generation is to learn the underlying distribution from a dataset of graphs $\mathcal{G} = \{G_1, \dots, G_n\}$ in order to synthesize new, valid samples. We focus on graphs with categorical node and edge attributes, a common setup in molecular design (Vignac et al., 2023). Formally, we define a graph as a tuple $G = (V, E, \mathbf{x}, \mathbf{e})$, where V is the set of nodes, $E \subseteq V \times V$ is the set of edges, and $\mathbf{x} : V \rightarrow \mathcal{X}$ and $\mathbf{e} : E \rightarrow \mathcal{E}$ assign attributes from discrete label sets \mathcal{X} and \mathcal{E} , respectively. The task is then to learn a parameterized model $P_\theta(G)$ that approximates the true data distribution and to use it for generating novel graphs $G' \sim P_\theta(\cdot)$.

Prevailing approaches fall into two families: (i) diffusion models, which learn $P_\theta(G)$ by minimizing a divergence (typically KL) and generate graphs via computationally inefficient, iterative denoising (Yang et al., 2024); and (ii) fragment-based methods that assemble graphs from pre-defined substructures using heuristic search or hard-coded

rules. Despite strong generative performance, these models typically offer limited user-steerable control and do not provide explicit, verifiable satisfaction of real-world design constraints.

2.2. Constraint Satisfaction Problem Solving and SMT Solving

The deterministic assembly stage of our framework is formulated as a Constraint Satisfaction Problem (CSP), necessitating a tool with formal guarantees. For this, we turn to Satisfiability Modulo Theories (SMT) solvers. While any off-the-shelf SMT solver could be employed, we choose Z3 (de Moura & Bjørner, 2008) as it is considered state-of-the-art in performance and reliability.

A theory T in first-order logic defines a set of symbols (e.g., constants like 0, functions like +) and axioms that constrain their interpretation (e.g., the theory of linear integer arithmetic, T_{LIA}). An SMT solver’s task is to determine if a given quantifier-free first-order formula ϕ is *T-satisfiable*—that is, if there exists a model that satisfies both the axioms of T and the formula ϕ . In this work, the formula ϕ will be the encoding of constraints used to assemble a valid graph from a proposed blueprint.

The problem is typically defined by a logical formula ϕ over a set of variables $Z = \{z_1, \dots, z_m\}$, where each variable z_i has a corresponding domain D_i . The formula is a conjunction of constraints

$$C = \{c_1, \dots, c_n\} : \quad \phi := \bigwedge_{j=1}^n c_j(Z_j), \quad Z_j \subseteq Z. \quad (1)$$

A solution is a *model* M , which is an interpretation mapping each variable to a value in its domain, $M : Z \rightarrow D$, such that the formula is satisfied ($M \models \phi$). The solver returns one of two outcomes:

- SAT (Satisfiable): A valid model M exists and is returned.
- UNSAT (Unsatisfiable): The solver proves that no such model exists.

The model M returned by the solver on a SAT result provides the deterministic instructions for constructing a valid graph. We detail our specific constraint encoding ϕ in Section 3.2.

3. The NSGGM Framework

NSGGM treats graph generation as a compositional task, analogous to building with modular components. Our method first decomposes existing molecule scaffolds into a vocabulary of fundamental pieces. A new, valid graph is

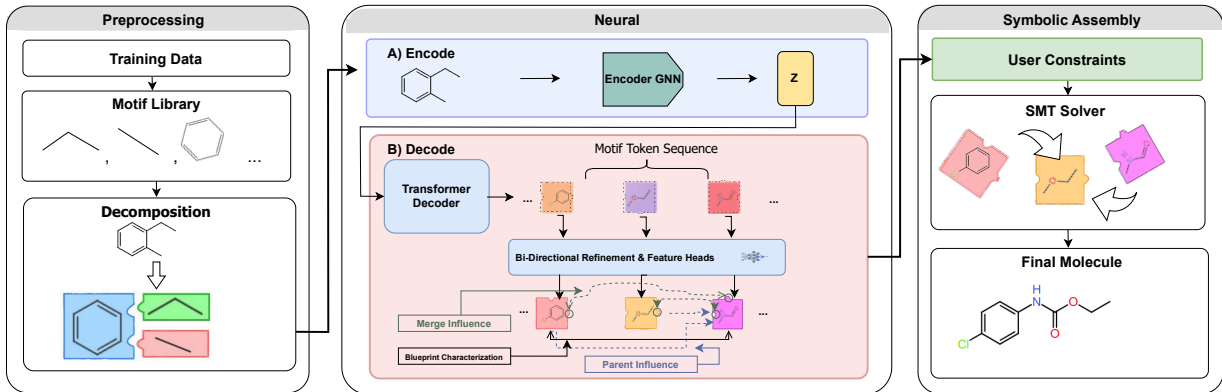


Figure 1. An overview of the NSGGM framework.

then created by sampling from this vocabulary and assembling the pieces while adhering to symbolic assembly constraints and neural guidance. Figure 1 provides an overview of this neuro-symbolic framework.

3.1. Decomposition and Vocabulary

Structural partitioning Our decomposition leverages the graph’s cycle structure, akin to fragment-based methods (e.g., Jin et al., 2018; Mercado et al., 2021). For $G = (V, E)$, we compute a minimum cycle basis $\mathcal{C}(G) = \{c_1, \dots, c_p\}$ and split edges into

$$E_C = \bigcup_{j=1}^p E(c_j), \quad E_A = E \setminus E_C. \quad (2)$$

Let $G_A = (V, E_A)$. We define the set of *primitives* as

$$\mathcal{P}(G) := \mathcal{C}(G) \cup \text{Components}(G_A), \quad (3)$$

and enumerate $\mathcal{P}(G) = \{P_i = (V_i, E_i)\}_{i=1}^m$. By construction, these primitives form an *overlapping cover* of G , i.e., $\bigcup_i V_i = V$ and $\bigcup_i E_i = E$. We make overlaps explicit via

$$V_{\text{sh}} = \bigcup_{i \neq j} (V_i \cap V_j), \quad E_{\text{sh}} = \bigcup_{i \neq j} (E_i \cap E_j). \quad (4)$$

For the acyclic part, we further refine $\text{Components}(G_A)$ into recurring *tree motifs* (Appendix A). Compared to Jin et al. (2018), which uses single edges (plus rings) as acyclic clusters, we admit multi-edge tree motifs and equip them with explicit slot interfaces; overlaps $(V_{\text{sh}}, E_{\text{sh}})$ are reconciled during assembly by slot matching, without requiring explicit projection maps.

Molecular interface characterization To enable guided reassembly, we define interfaces over node and edge *bond-type slot assignments*, σ_V and σ_E , enriched with chemistry-aware attributes.

Let \mathcal{E} be the set of element types and \mathcal{B} the set of bond orders (e.g., $\mathcal{B} = \{1, 2, 3\}$ for single/double/triple), and define $\text{elem}: V \rightarrow \mathcal{E}$, $\text{val}: V \rightarrow \mathbb{N}$, and $\text{bo}: E \rightarrow \mathcal{B}$. For a token g_i , define the residual bond-type capacities at v as

$$r_{i,b}(v) := \text{val}(v) - \sum_{e \in E_i(v)} \text{bo}(e)$$

restricted to bond order $b \in \mathcal{B}$ and set the node slot assignment to

$$\sigma_V(v, g_i) = (\text{elem}(v), \text{val}(v), (r_{i,b}(v))_{b \in \mathcal{B}}), \\ r_{i,b}(v) \geq 0 \quad \forall b \in \mathcal{B}.$$

where $E_i(v)$ are bonds incident to v within token g_i .

For shared internal bonds, we record their bond order:

$$\sigma_E(e, g_i) := \text{bo}(e), \quad e \in E_i \cap E_{\text{sh}}.$$

We prove that Structural Partitioning yields an overlapping cover of G with cycles and tree components as primitives, and uniquely determined interface slots (Proposition B.1, Appendix B.1).

Vocabulary and blueprint A *motif* is a subgraph type $g \in \mathcal{V}$ (up to isomorphism), where the global vocabulary \mathcal{V} is discovered from the training set \mathcal{G} . For each primitive occurrence $P_i = (V_i, E_i) \in \mathcal{P}(G)$, we assign its motif type $g_i \in \mathcal{V}$ and let the neural model select an *interface characterization*

$$s_i = (\sigma_V^i, \sigma_E^i),$$

A concrete assignment of the interface-slot functions, restricted to characterizations observed in the training data. We represent the resulting annotated instance by $t_i = (g_i, s_i)$. The *blueprint* for G is the multiset of annotated instances

$$S_G = \{t_i\}_{i=1}^m, \quad (5)$$

where $m := |\mathcal{P}(G)|$ is the number of primitive occurrences in G .

3.2. Assembly Constraints for Graph Synthesis

Given a blueprint $S' = \{t_1, \dots, t_k\}$ of slotted primitives $t_i = (g_i, s_i)$, determine a *merging of nodes* across primitives such that (i) matched node and edge slots are compatible (type-equality and residual-capacity satisfaction), and (ii) the induced identifications yield a consistent graph G' respecting all connections. This is encoded as an SMT constraint-satisfaction problem with variables for node identifications and constraints enforcing slot compatibility and global consistency.

Decision variables Let $V_{\text{slots}} = \bigcup_i V_i^{\text{slot}}$ be the set of all node-slot atoms in the blueprint. For every pair of distinct primitives $i \neq j$ and atoms $u \in V_i^{\text{slot}}, v \in V_j^{\text{slot}}$, we introduce a Boolean merge variable

$$m_{u,v} \in \{0, 1\},$$

interpreted as $m_{u,v} = \text{True} \iff u$ and v are merged in G' . Edge-slot sharing is realized implicitly via endpoint merges: two edge-slot copies $(u, v) \in E_i^{\text{slot}}$ and $(u', v') \in E_j^{\text{slot}}$ are considered *edge-merged* iff their endpoints are merged in a consistent orientation satisfying the hard constraints outlined below and in Appendix B.2

Hard constraints (ϕ_{hard}) Hard constraints are inviolable and enforce topological integrity and interface consistency. Let the internal (within-primitive) bond-order degree of an atom $u \in V_i$ be $\text{deg}_i(u)$. We impose: $\forall u, v$,

$$\begin{aligned} m_{u,v} \Rightarrow & \quad u \in V_i, v \in V_j \quad \text{for some } i \neq j, \\ & \quad m_{u,v} \Rightarrow \text{elem}(u) = \text{elem}(v), \\ & \quad \text{deg}_i(u) + \text{deg}_j(v) \leq \text{cap}(\text{elem}(u)). \end{aligned}$$

For edge merges, this requires $m_{u,v}$ and $m_{nu,nv}$ to both be true, where nu, nv are neighbours to u, v from the respective subgraphs, that is, they form edges $e = (u, nu) \in t_i$ and $e' = (v, nv) \in t_j, i \neq j$. We impose that may be merged only if they (i) have the $\text{bo}(e) = \text{bo}(e')$, and (ii) their endpoints are merged consistently, that is $m_{u,v} = m_{nu,nv} = \text{True}$ with the fact that $\text{bo}(e)$ can be subtracted from valency cap and $e \in E_i^{\text{slot}}$ and $e' \in E_j^{\text{slot}}$. See details in Appendix B.2.

Neural guidance (Soft constraints (ϕ_{soft})) We use weighted Max-SMT to satisfy all hard constraints while maximizing soft rewards. Soft constraints are used to encourage connectivity, that is, encourage subgraph tokens to connect to each other or in certain ways so that the final result is not fragmented. For implementation details see Appendix B.3

(i) *Neural parent guidance (decoder tree)*. If the decoder predicts a parent primitive for each child, we reward connecting each child to its predicted parent.

Correctness guarantees. For any blueprint S' , there exists a feasible assignment that reassembles each training graph from its own tokens (Corollary B.2). Moreover, any assignment satisfying ϕ_{hard} yields a well-defined simple graph; in the molecular case it also enforces element consistency, unique bond orders, and exact valency (Theorem B.3). Together, these imply correctness-by-construction and completeness for training graphs (Corollary B.4). Proofs are provided in Appendix B.1.

User constraints (ϕ_{user}) Let s denote the solver decision variables introduced by our assembly encoding (e.g., merge variables $\{m_{u,v}\}$ and, when applicable, bond/order variables). We optionally introduce auxiliary variables a that represent higher-level, user-facing properties of the assembled graph (e.g., indicators or counts), together with a definitional theory $\phi_{\text{aux}}(s, a)$ that makes each such property a function of s . Users may then supply an additional constraint formula $\phi_{\text{user}}(s, a)$ written in the same quantifier-free SMT theory as our encoding.

User constraints never weaken hard constraints: the final hard feasibility formula is

$$\Phi_{\text{hard}}(s, a) := \phi_{\text{hard}}(s) \wedge \phi_{\text{aux}}(s, a) \wedge \phi_{\text{user}}(s, a).$$

Thus ϕ_{user} can only restrict the feasible set (or make it empty). The solver returns either (i) SAT with a model M , from which we deterministically decode the output graph G' , or (ii) UNSAT, certifying that no graph satisfies all hard requirements. The full implementation of these constraints in the solver is given in the Appendix B.3

3.3. Neural Proposals

Under our decomposition, each molecule, \mathcal{G} , is represented by a finite sequence of motif tokens, $\mathcal{T} = (g_1, \dots, g_n)$, from the global *vocabulary* \mathcal{V} . We employ a VAE with a GNN encoder that operates on a *motif graph* representation of a molecule, G . Given a primitive decomposition $\mathcal{P}(G) = \{P_i\}_{i=1}^m$, we define the motif graph $H(G) = (\mathcal{P}(G), E_H)$ where $(P_i, P_j) \in E_H$ iff P_i and P_j overlap (i.e., share at least one node/edge) or are connected by an edge in G . The encoder maps $H(G)$ to a latent code z . We model the conditional $P(\mathcal{T}|z)$ auto-regressively, followed by a bidirectional refinement network that predicts *blueprint* interface characterizations (s_1, \dots, s_n) . The network classifies the *blueprint* of each token g_i through $P(k|\mathcal{T})$ to select the top blueprint prototype from Ω_t , a fixed set of top- K *blueprint* variants observed for that scaffold during training.

Scaffolds as sequences Let a *scaffold proposal sequence* be an ordered sequence $S = (g_1, \dots, g_k, \langle \text{eos} \rangle)$. Conditioned on the latent z , we parametrize the marginal likeli-

hood as:

$$p_\theta(S); =; \int p(\mathbf{z}) \cdot \prod_{\ell=1}^{k+1} P_\theta(g_\ell \mid g_{<\ell}, \mathbf{z}), d\mathbf{z}, \quad g_{k+1} \equiv \langle \text{eos} \rangle. \quad (6)$$

Hierarchical graph encoder We define a GNN encoder f_θ that maps a molecule G to an embedding in \mathbb{R}^d by operating on a coarse-grained decomposition graph $H(G) = (\mathcal{P}(G), E_H)$. Nodes of $H(G)$ correspond to primitive occurrences $P_i = (V_i, E_i) \in \mathcal{P}(G)$ and are featurized by their motif type $g_i \in \mathcal{V}$ (Section 3.1). We define an edge $(P_i, P_j) \in E_H$ whenever P_i and P_j overlap in G , and annotate it with a binary relation $r_{ij} \in \{0, 1\}$, indicating whether the overlap includes a shared edge ($r_{ij} = 1$) or only shared nodes ($r_{ij} = 0$).

The latent z is sampled from the global sum-pooling of the final representation $h_G = \sum h_i^{(L)}$:

$$z \sim \mathcal{N}(\mu_\phi(\mathbf{h}_G), \sigma_\phi^2(\mathbf{h}_G)) \quad (7)$$

Vocabulary decoder: We model the autoregressive generation of the motif sequence $\mathcal{T} = (g_1, \dots, g_L)$ by approximating $P(\mathcal{T} \mid z)$ via a causal Transformer decoder. Given time step $g_{<\ell}$ and latent z .

3.4. Neural Guidance (Refinement)

Post-decoder refinement Let the hidden decoder states $\{\mathbf{h}_\ell^{\text{dec}}\}_{\ell=1}^L \subset \mathbb{R}^d$ conditioned on the partial token sequence \mathcal{T} and latent z . A bidirectional Transformer encoder ϕ_{post} refines these states to $\mathbf{H} = \{\mathbf{h}_\ell\}_{\ell=1}^L$:

$$\mathbf{H} = \phi_{\text{post}}(\mathbf{H}^{\text{dec}}), \quad \mathbf{h}_\ell \in \mathbb{R}^d.$$

We then model three conditional distributions at each position ℓ that acts like *neural guidance* during assembly.

Blueprint characterization head Recall that each blueprint instance is $t_\ell = (g_\ell, s_\ell)$, where s_ℓ is an interface characterization (Section 3.1). We define a discrete characterization vocabulary

$$\mathcal{V}_b := \bigcup_{g \in \mathcal{V}} \mathcal{S}(g),$$

where $\mathcal{S}(g)$ is the finite set of characterizations for motif type g observed in the training data. At position ℓ , the decoder predicts s_ℓ from the hidden state \mathbf{h}_ℓ via

$$p(s_\ell \mid g_{\leq \ell}, z) = \text{softmax}(\mathbf{W}_b \mathbf{h}_\ell + \text{mask}(g_\ell)),$$

where $\text{mask}(g_\ell)$ restricts the softmax support to $\mathcal{S}(g_\ell) \subseteq \mathcal{V}_b$.

Merge-influence head To further guide assembly, we predict a binary *merge-type* indicator $m_\ell \in \{0, 1\}$ at each position ℓ , where $m_\ell = 0$ denotes a *node-merge* operation and $m_\ell = 1$ denotes an *edge-merge* operation. We model this as a Bernoulli distribution parameterized by the refined state \mathbf{h}_ℓ .

Parent-influence head We predict a parent index $\pi_\ell \in \{1, \dots, L\} \setminus \{\ell\}$ for each position ℓ (self-parenting is disallowed). We compute bilinear attention scores

$$s_{\ell j} = d^{-1/2} (\mathbf{h}_\ell \mathbf{W}_Q) (\mathbf{h}_j \mathbf{W}_K)^\top,$$

and normalize over all valid choices $j \neq \ell$:

$$P(\pi_\ell = j \mid \mathcal{T}, z) = \frac{\exp(s_{\ell j})}{\sum_{p \neq \ell} \exp(s_{\ell p})}, \quad j \neq \ell.$$

3.5. Training Details

Decomposition Each molecule is decomposed as described in Section 3.1. Then, each interface, h , is mapped to: (1) a *structure token* t_ℓ given by a structural Weisfeiler-Lehman (WL) hash h_{struct} (looked up in a fixed vocabulary), and (2) a *blueprint characterization variant* hash h_{meta} capturing interface/slot instantiation. For every h_{struct} , we maintain the top- K most frequent metadata variants and supervise a categorical target $t'_\ell \in \{1, \dots, K\}$ whenever the ground-truth h_{meta} falls in this candidate set (otherwise the position is ignored via masking).

Two-stage decoding Decoding scaffold proposals happens in two stages: (1) an autoregressive Transformer decoder generates scaffold-token sequence \mathcal{T} conditioned on latent z , (2) a bidirectional Transformer encoder refines the token-level representations through the *full* teacher-forced sequence to predict global structural annotations that guides downstream assembly.

Objective We aim to maximize the marginal log-likelihood of the observed outputs $y := (\mathcal{T}, \pi_{1:L}, m_{1:L}, t'_{1:L})$ under both training modes: full-molecule reconstruction and scaffold-conditioned generation:

$$\max_{\theta, \phi} \mathbb{E}_{(G) \sim \mathcal{D}} \left[\int p_\theta(y \mid z) p_\phi(z \mid G) dz \right], \quad (8)$$

which is intractable to optimize directly; in practice we maximize a variational lower bound (ELBO). The full ELBO and complete training are given in Appendix B.4.

4. Experiments and Results

We evaluate our neurosymbolic approach along two objectives: (i) distribution fidelity and competitive performance

Table 1. Unconditional de novo molecule generation on GuacaMol.

Model	Valid \uparrow	Unique \uparrow	FCD \uparrow	KL \uparrow	Novel \uparrow
MoLER (2022)	100.0	100.0	62.5	96.4	99.1
MiCAM (2023)	100.0	99.4	73.1	98.9	98.6
DiGress (2023)	85.2	100.0	68.0	92.9	99.9
LSTM	95.9	100.0	91.3	99.1	91.2
DISCO-GT (2024)	100.0	86.6	59.7	92.6	99.9
NSGGM (ours)	100.0 \pm 0.0	100.0 \pm 0.0	86.1 \pm 0.4	95.5 \pm 0.1	98.9 \pm 0.0

Table 2. Unconditional de novo molecule generation on MOSES. We report standard MOSES benchmark metrics. — indicates that the metric is not reported in the original paper.

Model	Valid \uparrow	Unique \uparrow	Novel \uparrow	Filters \uparrow	FCD \uparrow	SNN \uparrow	Scaf \uparrow
JT-VAE (2018)	100.0	100.0	99.9	97.8	81.8	0.53	10.0
MoLER (2022)	100.0	99.9	97.1	—	85.2	—	—
DiGress (2023)	85.7	100.0	95.0	97.1	78.8	0.52	14.8
GRAPHINVENT (2021)	96.4	99.8	—	95.0	78.3	0.54	12.7
DISCO-GT (2024)	88.3	100.0	97.7	95.6	74.9	0.50	15.1
NSGGM (ours)	100.0 \pm 0.0	100.0 \pm 0.0	94.4 \pm 0.3	97.1 \pm 0.1	82.3 \pm 0.3	0.5 \pm 0.0	11.2 \pm 0.1

Table 3. Unconditioned molecule generation on QM9 implicit hydrogens. — indicates that the metric is not reported in the original paper.

Model	Valid \uparrow	Unique \uparrow	FCD \uparrow	KL \uparrow
JT-VAE (2018)	100.0	54.9	58.8	89.1
MoLER (2022)	100.0	94.0	93.1	96.9
LO-ARM-ST-SEP (2025)	99.9	98.9	95.3	—
DiGress (2023)	99.0 \pm 0.1	96.2 \pm 0.1	—	—
UNIGEM (2025)	95.0 \pm 3.1	98.1	—	—
MiCAM (2023)	100.0	93.2	94.5	98.0
DISCO-GT (2024)	99.3 \pm 0.6	99.5	—	—
NSGGM (ours)	100.0 \pm 0.0	96.1 \pm 0.2	94.7 \pm 0.4	94.0 \pm 1.0

under unconstrained generation on small and large scale benchmarks, and (ii) exploratory robustness under hard structural constraints at inference time (i.e. logical and scaffold constraints). Accordingly, we test whether exact symbolic constraints can be enforced without costly retraining while preserving generative signals from the neural mode for exploration within the constrained space.

4.1. Unconstrained Generation

Setup We evaluate on QM9 (Wu et al., 2018), MOSES (Polykovskiy et al., 2020), and GuacaMol (Brown et al., 2019); dataset details are in Appendix C. For MOSES and GuacaMol, we use the official training, validation, and test splits and 80/10/10 split for QM9. Unless stated otherwise, all results are averaged over three runs, each generating 10k molecules, and we report mean and standard deviation. Also, we report generation throughput and hardware in Appendix D.1.

In our benchmarks, for distribution fidelity, we use Fréchet ChemNet Distance (FCD) (Preuer et al., 2018) and KL Divergence (KL). KL measures how different the property distributions of generated molecules are from the training data. FCD measures the similarity between generated and real molecules using ChemNet embeddings. Additionally, we evaluate on standard fidelity-focused metrics like *Validity* (Correctness) and *Unique* (Uniqueness).

Small scale unconstrained generation We report QM9 with the standard metrics: *Validity*, *Unique* (Uniqueness), FCD, and KL in Table 3.

Large-scale generation We evaluate on MOSES (Polykovskiy et al., 2020) and GuacaMol (Brown et al., 2019). For GuacaMol, we report *Validity*, *Uniqueness*, *Novelty*, and standard distributional metrics including FCD and KL divergence in Table 1. For MOSES in Table 2, we report FCD, and standard MOSES evaluation metrics including *Filters*, *SNN*, and *Scaffold similarity* (*Scaf*) on the *TestSF* split which is made of separate scaffolds not seen during training. *Filters* measure the percentage of generated molecules that pass the same chemical constraints of the test set, *SNN* measures the similarity to the nearest molecule using Tanimoto similarity, and *scaffold similarity* represents the Bemis–Murcko scaffold overlap with test molecules.

Analysis As shown in Tables 3, 1, 2, NSGGM demonstrates consistent strong behaviour across the increasing scales. On all benchmarks, NSGGM achieves 100% validity by construction and strong distributional alignment,

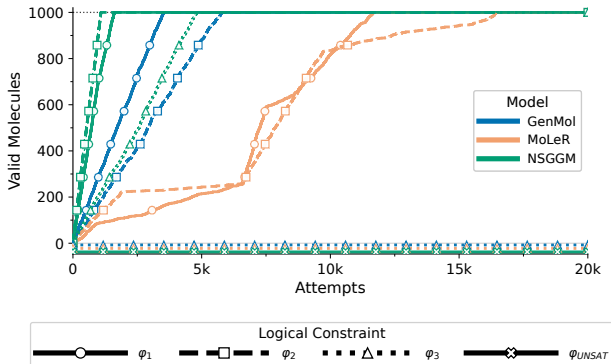


Figure 2. Sample efficiency under logical constraints: cumulative number of constraint-satisfying molecules (up to 1000) versus the number of generation attempts. Colours denote model type and markers/linestyles denote constraints φ_1 – φ_{UNSAT} (with φ_{UNSAT} unsatisfiable by construction). We only plot first 20K attempts for readability as curves beyond 20K are flat.

confirming the importance of the neural component in guiding the symbolic solver. On GuacaMol, NSGGM achieves competitive normalized FCD, outperforming most baselines while maintaining high novelty, indicating that symbolic assembly does not degrade distributional metrics at scale. On MOSES, NSGGM achieves high filter pass rates and low FCD with strong nearest-neighbor similarity (SNN), demonstrating its ability in remaining close to the training distributional despite symbolic structural enforcement.

Table 4. NSGGM ablations on GuacaMol. **Full**: complete neuro-symbolic pipeline (neural proposal + neural refinement + symbolic solver). **W/o neural guidance**: remove the neural refinement/guidance stage; the solver operates on coarse/high-level proposals. **W/o solver**: remove the symbolic solver; generate directly off of neural component.

Variant	Valid \uparrow	FCD \uparrow
Full	100.0 \pm 0.0	86.1 \pm 0.4
W/o neural guidance	100.0 \pm 0.0	46.0 \pm 1.2
W/o solver	58.4 \pm 2.4	30.0 \pm 1.1

Ablation To further our findings, we perform ablations on GUACAMOL in Table 4 to quantify how much the performance depends on the neural versus the symbolic solver component. From the table, removing the neural guidance component substantially degrades distributional match (FCD), while removing the solver greatly reduces both validity and FCD as local connectivity signal is lost.

4.2. Logical Constraint Satisfaction

Next, we evaluate NSGGM on four synthetic, chemistry-inspired, logical constraints ($\rho_1, \rho_2, \rho_3, \rho_{UNSAT}$) spanning high, low, and zero training-data support, designed to test whether NSGGM can produce chemically valid molecules that exactly satisfy increasingly difficult specifications.

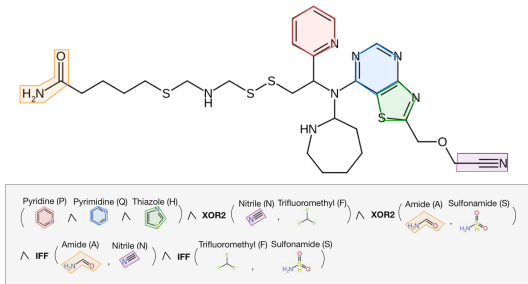


Figure 3. Example generated molecule satisfying φ_3

Baselines We compare against MOLER (Maziarz et al., 2022) and GENMOL (Lee et al., 2025) as two recent controllable generators that can be seeded/conditioned on structural conditions, while many other models would require task-specific fine-tuning to support comparable control.

All neural components are trained on GuacaMol. To obtain a comparable baseline for purely neural generators, we use a *generate-and-filter* evaluation strategy: we sample candidate molecules from baseline models (biased sampling by seeding with molecules from training set that satisfy the corresponding constraint) and apply exact logical constraint checking, rejecting samples that violate it. For all neural models, we give a sampling budget of **50K** molecule attempts. For NSGGM, logical constraints are applied only at generation time via SMT-based symbolic verification. We **do not** fine-tune the model on any of the objectives and consider the *UNSAT* case for our model to count as a *fail* for a fair comparison (otherwise NSGGM will be trivially perfect).

Constraint semantics Each constraint is a propositional formula over scaffold-presence predicates designed to test non-local logical coupling (i.e., XOR/IFF/AND), varying support/coverage (high vs. low vs. near-zero), and correct UNSAT detection. We give an annotated example satisfying molecule for constraint φ_3 from our model in Figure 3. Full specifications of constraints $\{\varphi_1, \varphi_2, \varphi_3, \varphi_{UNSAT}\}$ are provided in Appendix D.3.

Results Figure 2 shows the sample efficiency under increasing restrictive logical constraints. NSGGM achieves greater satisfaction efficiency on φ_1 and φ_2 within the fixed budget (exceeding 50% efficiency), while neural baselines lag substantially. Constraint φ_3 reveals a major distinction: since φ_3 has no satisfying molecules in the training set, unconstrained generation with filtering becomes ineffective where baseline models obtain zero satisfying samples within the sampling budget. On the other hand, NSGGM still achieves a non-trivial satisfaction rate (about 25%) thanks to the exact symbolic enforcement rather than relying on rare hits. Finally, we evaluate only NSGGM on φ_{UNSAT} ,

Table 5. Hard scaffold-constrained generation results across scaffold sets Σ_1 – Σ_3 . NSGGM achieves perfect validity and novelty while delivering leading uniqueness.

Scaf.	Model	Validity \uparrow	Uniqueness \uparrow	Novelty \uparrow
Σ_1	MOLEr	100.0	93.2	100.0
	GENMOL	82.4	75.1	70.3
	NSGGM (Ours)	100.0	98.9	100.0
Σ_2	MOLEr	100.0	93.1	93.8
	GENMOL	81.5	70.4	60.2
	NSGGM (Ours)	100.0	91.5	100.0
Σ_3	MOLEr	100.0	96.6	100.0
	GENMOL	82.1	83.3	47.8
	NSGGM (Ours)	100.0	99.8	100.0

where it produced no satisfying result, consistent transparent, interpretable, and formal constraint checking.

Overall, these results showcase the difficulty of enforcing global, interpretable logical structure when sampling alone, and reveals how a SMT-based verification offers a transparent and auditable approach in enforcing exact constraint satisfaction, an important property in controlled molecule generation environments where requirements must be stated and checked explicitly.

4.3. Scaffold-Constrained Generation

Next, we evaluate hard constrained scaffold generation, where each molecule must contain a fixed scaffold as a connected subgraph or as part of a logical constraint. This can be represented as a hard structural constraint in symbolic logic and enforced by our symbolic SMT-solver rather than being approximated via rewards. Unlike unconstrained generation, under hard constraints, the valid output space is fundamentally restricted, so we will focus on constraint satisfaction and exploratory metrics such as *Uniqueness* and *Novelty*. Similar to the logical constraints evaluation, we compare against MOLEr and GENMOL as they can explicitly support scaffold / fragment-conditioned decoration. As all baselines and NSGGM natively enforce the provided scaffold, scaffold retention is 100% across all methods, so we omit it from our results and focus on validity, uniqueness, and novelty.

We evaluate by generating 1000 molecules for each core scaffolds, specifically Quinoline (Σ_1) (PubChem CID 7047), Phenazine (Σ_2) (PubChem CID 4757), and a large drug-like core scaffold (Σ_3) (PubChem CID 154108) as fixed scaffolds. As shown in Table 5, NSGGM and MOLEr achieve 100% validity by construction. NSGGM outperforms MOLEr on uniqueness for Σ_1 and Σ_3 while remaining competitive for Σ_2 . MOLEr is a strong baseline as it is scaffold-seeded by design, yet NSGGM still leads in scaffold exploration, which we attribute to the tunable neural-solver balance: more solver dependence increases

exploration.

5. Related Work

Diffusion models have emerged as a dominant paradigm for graph and molecular generation, focusing on unconstrained generation and task optimization, from continuous formulations that corrupt adjacency/node representations with Gaussian noise and denoising them back to graphs (Niu et al., 2020; Jo et al., 2022) to discrete diffusion that operates directly over categorical node and edge attributes (Vignac et al., 2023; Haefeli et al., 2023). Some recent diffusion works further improve controllability through conditioning and guidance mechanisms by activating property-aware objectives late in the schedule (after scaffold emerges) (Lee et al., 2025; Feng et al., 2025). Concurrently, Haefeli et al. (2023) study unattributed graphs and also find discrete diffusion effective. While highly effective for distribution learning, constraints in diffusion-based generators are typically incorporated implicitly, as a result, they generally do not provide formal guarantees for arbitrary user-specified global structural or logical constraints.

Beyond diffusion, VAEs, GANs, and flows have been explored (Zhu et al., 2022; Madhawa et al., 2019; Liu et al., 2018b; Luo et al., 2021), but they typically lag strong autoregressive models (Liao et al., 2019; Mercado et al., 2021) and motif-based methods (Jin et al., 2020a; Maziarz et al., 2022) that encode domain knowledge. While these models can support practical conditioning i.e. MOLEr and GENMOL can be seeded/conditioned on structural inputs, their control is expressed through conditioning variable and guidance examples which makes it difficult to (i) explicitly enforce coupled non-local logical statements exactly and (ii) certify and interpret infeasibility for UNSAT specifications.

6. Conclusion

We introduce Neuro-Symbolic Graph Generative Modeling (NSGGM), a neuro-symbolic framework for molecule generation that combines scaffold/interaction proposals with SMT-based symbolic assembly. This results in strong generative quality while allowing for explicit, interpretable constraints with SAT/UNSAT detection and correctness-by-construction under encoded rules; we also introduce a *Logical-Constraint Molecular Benchmark* to evaluate strict and explicit rule compliance. While explicitly specifying constraints in logic can be fragile and may not capture under-specified preferences, we believe this work is an important step in bringing transparent, auditable control to a field dominated by black-box neural generative models, and we hope it motivates future works that better balance flexibility with verification and interpretability.

Impact Statement

This work introduces NSGGM, a framework that bridges deep learning with formal symbolic reasoning to ensure structural and chemical validity in molecular generation. By ensuring that generated molecules are correct by construction via an SMT solver, NSGGM significantly reduces the risk of AI-generated hallucinations—chemically impossible or unstable structures that often consume substantial laboratory resources to disprove. This advancement accelerates the pipeline from computational design to experimental validation, potentially lowering the costs and timelines associated with developing life-saving therapeutics. Furthermore, the introduction of the *Logical-Constraint Molecular Benchmark* promotes a necessary shift toward verifiable AI in highly regulated sectors such as pharmacology and materials science. By allowing researchers to define explicit safety boundaries and enforce strict hard-rule satisfaction, this approach fosters greater trust among domain experts and regulatory bodies, ensuring that AI-driven designs comply with rigorous safety, ethical, and environmental standards.

References

- Amann, J., Blasimme, A., Vayena, E., Frey, D., Madai, V. I., and consortium, P. Explainability for artificial intelligence in healthcare: A multidisciplinary perspective. *BMC Medical Informatics and Decision Making*, 20(1):310, Nov 2020. doi: 10.1186/s12911-020-01332-6. URL <https://doi.org/10.1186/s12911-020-01332-6>.
- Asai, T., Arimura, H., Uno, T., and Nakano, S.-I. Discovering frequent substructures in large unordered trees. In *International Conference on Discovery Science*, pp. 47–61. Springer, 2003.
- Barrett, C. and Tinelli, C. Satisfiability modulo theories. In *Handbook of model checking*, pp. 305–343. Springer, 2018.
- Brockschmidt, M., Allamanis, M., Gaunt, A. L., and Polozov, O. Generative code modeling with graphs. In *7th International Conference on Learning Representations, ICLR 2019, New Orleans, LA, USA, May 6-9, 2019*. OpenReview.net, 2019. URL <https://openreview.net/forum?id=Bke4KsA5FX>.
- Brown, N., Fiscato, M., Segler, M. H. S., and Vaucher, A. C. Guacamol: Benchmarking models for de novo molecular design. *Journal of Chemical Information and Modeling*, 59(3):1096–1108, 2019. doi: 10.1021/acs.jcim.8b00839. URL <https://pubs.acs.org/doi/10.1021/acs.jcim.8b00839>.
- Cao, N. D. and Kipf, T. Molgan: An implicit generative model for small molecular graphs. *CoRR*, abs/1805.11973, 2018. URL <http://arxiv.org/abs/1805.11973>.
- Chang, C., Shen, Y., Fan, S., Li, J., Zhang, S., Cao, N., Chen, Y., and Zhang, X. Lamagic: Language-model-based topology generation for analog integrated circuits. In *Forty-first International Conference on Machine Learning, ICML 2024, Vienna, Austria, July 21-27, 2024*. OpenReview.net, 2024. URL <https://openreview.net/forum?id=MjGCD8wk1k>.
- de Moura, L. M. and Bjørner, N. S. Z3: an efficient SMT solver. In Ramakrishnan, C. R. and Rehof, J. (eds.), *Tools and Algorithms for the Construction and Analysis of Systems, 14th International Conference, TACAS 2008, Held as Part of the Joint European Conferences on Theory and Practice of Software, ETAPS 2008, Budapest, Hungary, March 29-April 6, 2008. Proceedings*, volume 4963 of *Lecture Notes in Computer Science*, pp. 337–340. Springer, 2008. doi: 10.1007/978-3-540-78800-3_24. URL https://doi.org/10.1007/978-3-540-78800-3_24.

- Feng, S., Ni, Y., yan, L., Ma, Z.-M., Ma, W.-Y., and Lan, Y. UniGEM: A unified approach to generation and property prediction for molecules. In *The Thirteenth International Conference on Learning Representations*, 2025. URL <https://openreview.net/forum?id=Lb91pXwZMR>.
- Geng, Z., Xie, S., Xia, Y., Wu, L., Qin, T., Wang, J., Zhang, Y., Wu, F., and Liu, T.-Y. De novo molecular generation via connection-aware motif mining. In *The Eleventh International Conference on Learning Representations*, 2023. URL https://openreview.net/forum?id=Q_Jexl8-qDi.
- Haefeli, K. K., Martinkus, K., Perraudin, N., and Wattenhofer, R. Diffusion models for graphs benefit from discrete state spaces, 2023. URL <https://arxiv.org/abs/2210.01549>.
- Jin, W., Barzilay, R., and Jaakkola, T. S. Junction tree variational autoencoder for molecular graph generation. In Dy, J. G. and Krause, A. (eds.), *Proceedings of the 35th International Conference on Machine Learning, ICML 2018, Stockholmsmässan, Stockholm, Sweden, July 10-15, 2018*, volume 80 of *Proceedings of Machine Learning Research*, pp. 2328–2337. PMLR, 2018. URL <http://proceedings.mlr.press/v80/jin18a.html>.
- Jin, W., Barzilay, R., and Jaakkola, T. Hierarchical generation of molecular graphs using structural motifs. In *Proceedings of the 37th International Conference on Machine Learning (ICML)*, 2020a. URL <https://arxiv.org/abs/2002.03230>.
- Jin, W., Barzilay, R., and Jaakkola, T. S. Hierarchical generation of molecular graphs using structural motifs. In *Proceedings of the 37th International Conference on Machine Learning, ICML 2020, 13-18 July 2020, Virtual Event*, volume 119 of *Proceedings of Machine Learning Research*, pp. 4839–4848. PMLR, 2020b. URL <http://proceedings.mlr.press/v119/jin20a.html>.
- Jo, J., Lee, S., and Hwang, S. J. Score-based generative modeling of graphs via the system of stochastic differential equations. 2022. URL <https://arxiv.org/abs/2202.02514>.
- Lee, S., Kreis, K., Veccham, S. P., Liu, M., Reidenbach, D., Peng, Y., Paliwal, S., Nie, W., and Vahdat, A. Genmol: A drug discovery generalist with discrete diffusion. In *Proceedings of the 42nd International Conference on Machine Learning*, 2025. URL <https://openreview.net/pdf?id=KM7pXWG1xj>.
- Liao, R., Li, Y., Song, Y., Wang, S., Nash, C., Hamilton, W. L., Duvenaud, D., Urtasun, R., and Zemel, R. S. Efficient graph generation with graph recurrent attention networks. 2019. URL <https://arxiv.org/abs/1910.00760>.
- Liu, Q., Allamanis, M., Brockschmidt, M., and Gaunt, A. L. Constrained graph variational autoencoders for molecule design. In Bengio, S., Wallach, H. M., Larochelle, H., Grauman, K., Cesa-Bianchi, N., and Garnett, R. (eds.), *Advances in Neural Information Processing Systems 31: Annual Conference on Neural Information Processing Systems 2018, NeurIPS 2018, December 3-8, 2018, Montréal, Canada*, pp. 7806–7815, 2018a. URL <https://proceedings.neurips.cc/paper/2018/hash/b8a03c5c15fcfa8dae0b03351eb1742f-Abstract.html>.
- Liu, Q., Allamanis, M., Brockschmidt, M., and Gaunt, A. L. Constrained graph variational autoencoders for molecule design. 2018b. URL <https://arxiv.org/abs/1805.09076>.
- Luo, Y., Yan, K., and Ji, S. Graphdf: A discrete flow model for molecular graph generation. 2021. URL <https://arxiv.org/abs/2102.01189>.
- Madhawa, K., Ishiguro, K., Nakago, K., and Abe, M. Graph-nvp: An invertible flow model for generating molecular graphs. 2019. URL <https://arxiv.org/abs/1905.11600>.
- Martinkus, K., Loukas, A., Perraudin, N., and Wattenhofer, R. Spectre: Spectral conditioning helps to overcome the expressivity limits of one-shot graph generators. In *Proceedings of the 39th International Conference on Machine Learning*, volume 162 of *Proceedings of Machine Learning Research*, pp. 15159–15202. PMLR, 2022. URL <https://proceedings.mlr.press/v162/martinkus22a.html>.
- Maziarz, K., Jackson-Flux, H. R., Cameron, P., Sirockin, F., Schneider, N., Stiefl, N., Segler, M., and Brockschmidt, M. Learning to extend molecular scaffolds with structural motifs. In *International Conference on Learning Representations (ICLR)*, 2022. URL <https://openreview.net/forum?id=nS6YyqpTT6y>.
- McKay, B. D. and Piperno, A. Practical graph isomorphism, ii. *Journal of symbolic computation*, 60:94–112, 2014.
- Mercado, R., Rastemo, T., Lindelöf, E., Klambauer, G., Engkvist, O., Chen, H., and Bjerrum, E. J. Graph networks for molecular design. *Mach. Learn. Sci. Technol.*, 2(2):25023, 2021. doi: 10.1088/2632-2153/ABCF91. URL <https://doi.org/10.1088/2632-2153/abcf91>.

- Niu, C., Song, Y., Song, J., Zhao, S., Grover, A., and Ermon, S. Permutation invariant graph generation via score-based generative modeling. 2020. URL <https://arxiv.org/abs/2003.00638>.
- Polykovskiy, D., Zhebrak, A., Sanchez-Lengeling, B., Golovanov, S., Tatanov, O., Belyaev, S., Kurbanov, R., Artamonov, A., Aladinskiy, V., Veselov, M., Kadurin, A., Johansson, S., Chen, H., Nikolenko, S., Aspuru-Guzik, A., and Zhavoronkov, A. Molecular sets (moses): A benchmarking platform for molecular generation models. *Frontiers in Pharmacology*, 11:565644, 2020. doi: 10.3389/fphar.2020.565644. URL <https://www.frontiersin.org/articles/10.3389/fphar.2020.565644>.
- Preuer, K., Renz, P., Unterthiner, T., Hochreiter, S., and Klambauer, G. Fréchet chemnet distance: A metric for generative models for molecules in drug discovery. *Journal of Chemical Information and Modeling*, 58(9):1736–1741, 2018. doi: 10.1021/acs.jcim.8b00234. URL <https://doi.org/10.1021/acs.jcim.8b00234>. PMID: 30118593.
- PubChem CID 154108. Dibenzo(c,f)(2,7)naphthyridine [cid 154108]. <https://pubchem.ncbi.nlm.nih.gov/compound/154108>. Accessed: 2026-01-29.
- PubChem CID 4757. Phenazine [cid 4757]. <https://pubchem.ncbi.nlm.nih.gov/compound/Phenazine>. Accessed: 2026-01-29.
- PubChem CID 7047. Quinoline [cid 7047]. <https://pubchem.ncbi.nlm.nih.gov/compound/Quinoline>. Accessed: 2026-01-29.
- Tarjan, R. Depth-first search and linear graph algorithms. *SIAM Journal on Computing*, 1(2):146–160, 1972. doi: 10.1137/0201010. URL <https://doi.org/10.1137/0201010>.
- Vignac, C., Krawczuk, I., Siraudin, A., Wang, B., Cevher, V., and Frossard, P. Digress: Discrete denoising diffusion for graph generation. In *The Eleventh International Conference on Learning Representations, ICLR 2023, Kigali, Rwanda, May 1-5, 2023*. OpenReview.net, 2023. URL <https://openreview.net/forum?id=UaAD-Nu86WX>.
- Wang, Z., Shi, J., Heess, N., Gretton, A., and Titsias, M. Learning-order autoregressive models with application to molecular graph generation. In *Forty-second International Conference on Machine Learning*, 2025. URL <https://openreview.net/forum?id=EY6pXIDi3G>.
- Wu, Z., Ramsundar, B., Feinberg, E. N., Gomes, J., Geniesse, C., Pappu, A. S., Leswing, K., and Pande, V. Moleculenet: A benchmark for molecular machine learning, 2018. URL <https://arxiv.org/abs/1703.00564>.
- Xu, Z., Qiu, R., Chen, Y., Chen, H., Fan, X., Pan, M., Zeng, Z., Das, M., and Tong, H. Discrete-state continuous-time diffusion for graph generation. In *The Thirty-eighth Annual Conference on Neural Information Processing Systems*, 2024. URL <https://openreview.net/forum?id=YkSKZEhIYt>.
- Yang, L., Zhang, Z., Song, Y., Hong, S., Xu, R., Zhao, Y., Zhang, W., Cui, B., and Yang, M. Diffusion models: A comprehensive survey of methods and applications. *ACM Comput. Surv.*, 56(4):105:1–105:39, 2024. doi: 10.1145/3626235. URL <https://doi.org/10.1145/3626235>.
- Zhu, Y., Du, Y., Wang, Y., Xu, Y., Zhang, J., Liu, Q., and Wu, S. A survey on deep graph generation: Methods and applications. 2022. URL <https://arxiv.org/abs/2203.06714>.

A. Further Decomposition of Acyclic Components

Algorithm 1 Refine Acyclic Components into Tree Motifs

Input: Graph $G = (V, E)$, acyclic edge set E_A , minimum support τ

Output: Tree-motif tokens \mathcal{T}_{tree} , residual fragments \mathcal{R}_{tree}

```

1 Function RefineAcyclic( $G, E_A, \tau$ )
2    $G_A \leftarrow (V, E_A)$  // Acyclic remainder subgraph
3    $\mathcal{C} \leftarrow \text{ConnectedComponents}(G_A)$   $\mathcal{T}_{tree} \leftarrow \emptyset, \mathcal{R}_{tree} \leftarrow \emptyset$ 
4   foreach  $C \in \mathcal{C}$  do
      // (1) BC decomposition and optional
      // path compression
5      $(\mathcal{B}, \mathcal{A}) \leftarrow \text{BlockCutDecompose}(C)$  // Blocks
       $\mathcal{B}$  and articulation points  $\mathcal{A}$ 
6      $\mathcal{B} \leftarrow \{\text{CompressDegTwoChains}(B) \mid B \in \mathcal{B}\}$  // Contract degree-2 chains within
      blocks
      // (2) Subtree enumeration and
      // canonicalization
7      $\mathcal{S} \leftarrow \bigcup_{B \in \mathcal{B}} \text{EnumerateSubtrees}(B)$ 
      // Enumerate candidate subtrees
      // (bounded depth/size)
8      $\mathcal{K} \leftarrow \{\text{CanonicalizeSubtree}(S) \mid S \in \mathcal{S}\}$  // Canonical forms for isomorphism
      handling
      // (3) Support counting (frequent
      // subtree mining)
9      $\text{supp}(\cdot) \leftarrow \text{CountSupport}(\mathcal{K}, \text{over all } C' \in \mathcal{C})$ 
       $\mathcal{F} \leftarrow \{K \in \mathcal{K} \mid \text{supp}(K) \geq \tau\}$  // Frequent
      patterns
      // (4) Tokenization and interface
      // slots
10    foreach  $K \in \mathcal{F}$  do
11       $g \leftarrow \text{RepresentativeSubtree}(K)$   $\sigma_V, \sigma_E \leftarrow$ 
       $\text{ComputeSlots}(g)$  // Node/edge slots
      for interfaces
12       $\mathcal{T}_{tree} \leftarrow \mathcal{T}_{tree} \cup \{\text{AssembleToken}(g, \sigma_V, \sigma_E)\}$ 
      // (5) Residuals: pieces not covered
      // by frequent motifs
13       $\mathcal{U} \leftarrow \text{MaximalUncoveredFragments}(C, \mathcal{F})$ 
      // after covering by  $\mathcal{F}$ 
14       $\mathcal{R}_{tree} \leftarrow \mathcal{R}_{tree} \cup \mathcal{U}$  // minimal trees /
      single edges
15  return  $\mathcal{T}_{tree}, \mathcal{R}_{tree}$ 

```

Each primitive $g_i \in \mathcal{P}(G)$ is a subgraph with node set V_i and edge set E_i . For the acyclic part, we refine connected components into recurring *tree motifs* using standard steps:

1. **BC decomposition:** Decompose at articulation points via a block-cut (BC) decomposition (Tarjan, 1972).
2. **Path compression:** Optionally compress degree-2 chains (a standard tree reduction).
3. **Frequent subtree mining:** Canonicalize subtrees and select frequent patterns by minimum support, follow-

ing frequent (sub)tree mining frameworks (Asai et al., 2003).

4. **Canonical labeling:** Use canonical labeling for isomorphism handling (McKay & Piperno, 2014).

Residual fragments that do not meet the support threshold remain as minimal trees (or single edges).

B. The NSGGM Method

B.1. Proofs

Proposition B.1 (Legitimacy of Structural Partitioning). *Let $G = (V, E)$ be any finite simple graph and let $\mathcal{C}(G) = \{c_1, \dots, c_p\}$ be a minimum cycle basis with edge sets $E(c_j)$. Define*

$$E_C = \bigcup_{j=1}^p E(c_j), \quad E_A = E \setminus E_C, \quad G_A = (V, E_A).$$

Let $\mathcal{P}(G) = \mathcal{C}(G) \cup \text{Components}(G_A)$ and enumerate $\mathcal{P}(G) = \{P_i = (V_i, E_i)\}_{i=1}^m$. Then:

- (i) $\{P_i\}$ is an overlapping cover of G : $\bigcup_i V_i = V$ and $\bigcup_i E_i = E$.
- (ii) Every P_i is either a simple cycle c_j or an induced connected acyclic subgraph (a tree component of G_A).
- (iii) If $v \in V_i \cap V_j$ or $e \in E_i \cap E_j$ for $i \neq j$, then the overlap corresponds to a genuine shared item of G (i.e., no spurious duplication).
- (iv) The blueprint $S_G = \{t_i\}_{i=1}^m$ with tokens $t_i = (P_i, \sigma_V|_{V_i}, \sigma_E|_{E_i})$ is well-defined; in particular, the slot maps σ_V, σ_E can be computed deterministically from G and $\mathcal{P}(G)$.

Proof. (i) By construction, $E = E_C \cup E_A$ and the union is disjoint. The family $\{E(c_j)\}_j$ covers E_C , while $\text{Components}(G_A)$ covers E_A . Hence $\bigcup_i E_i = E$. Since every edge's endpoints are included, $\bigcup_i V_i = V$ follows.

(ii) Each $c_j \in \mathcal{C}(G)$ is a simple cycle by definition of a cycle basis. Deleting E_C breaks all remaining cycles, so $G_A = (V, E_A)$ is acyclic; its connected components are trees.

(iii) If an item of G appears in two primitives, it is because that item is simultaneously part of a cycle and of another cycle (fused cycles) or it lies on the interface between a cycle and a tree component (or between fused cycles). In all cases, the overlap is an actual vertex/edge of G present in both subgraphs, not an artifact of the construction.

(iv) The slot assignments σ_V, σ_E are functions of local degrees in G and in each primitive, plus the fused/non-fused tag for cycle primitives (Section 3.1). Since these are determined from $(G, \mathcal{P}(G))$ with no ambiguity, t_i is uniquely defined for each P_i . \square

Corollary B.2 (Canonical Witness for Reassembly). *Let S_G be the blueprint of G from Proposition B.1. There exists an assignment $\{z_v\}_{v \in V_{\text{slots}}}$ (take z_v equal to the original global vertex ID of v) such that all hard constraints ϕ_{hard} in Section 3.2 are satisfied. Thus, every training graph admits a feasible assembly consistent with its own blueprint.*

Proof. Assign each local copy $v \in V_i$ the label $z_v := \text{id}_G(v)$ given by its vertex in G . Subgraph integrity holds because distinct local copies within the same primitive correspond to distinct vertices. Edge-slot matching holds since each shared edge of G appears with the same endpoints across primitives. Type-equality is immediate because copies refer to the same underlying item of G . Hence ϕ_{hard} is satisfied. \square

Theorem B.3 (Soundness of Assembly Under ϕ_{hard}). *Fix a blueprint $S' = \{t_1, \dots, t_k\}$ and any assignment $\{z_v\}_{v \in V_{\text{slots}}}$ that satisfies all hard constraints ϕ_{hard} of Section 3.2. Define an equivalence relation on slot-copies by $v \sim v' \iff z_v = z_{v'}$ and let $[v]$ denote its classes. Construct a graph $G' = (V', E')$ with $V' = \{[v] : v \in V_{\text{slots}}\}$ and with edges induced from primitive edges subject to edge-slot matching. Then:*

- (i) G' is a well-defined simple graph (no self-loops or parallel edges are introduced by merging).
- (ii) The embedding of each primitive P_i into G' is injective on its vertices and edges (subgraph integrity).
- (iii) If two local copies are merged, their discrete type fields match exactly (type consistency).

If, in addition, S' is molecular and the molecular hard clauses hold (element consistency, shared-edge order consistency, and exact valency balance), then:

- (iv) Every merged vertex in G' has element type well-defined and unique.
- (v) For each atom $u \in V'$, the total bond order of edges incident to u equals its prescribed valency; in particular, no deficit or surplus valence occurs.
- (vi) Any edge e occurring in multiple primitives has a single bond order in G' .

Consequently, G' is a topologically valid graph; in the molecular case it is chemically valid by construction.

Proof. (i) Define V' as the quotient by \sim . By *subgraph integrity*, two distinct vertices of the same primitive never merge, so a primitive cannot collapse onto itself. By *edge-slot matching*, whenever a structural edge is realized by merging endpoints from two primitives, its endpoints map to distinct equivalence classes (no self-loop). Parallel edges cannot arise because matched edge-slots are required to pairwise realize the same underlying adjacency; any duplicate realization would violate the matching condition.

(ii) Subgraph integrity is precisely the clause $z_{v_a} \neq z_{v_b}$ for distinct v_a, v_b of the same primitive; thus the primitive’s vertex set injects into V' and its edges map injectively into E' .

(iii) This is exactly the type-equality constraint: $z_{v_i} = z_{v_j} \implies \sigma_V^{\text{type}}(v_i) = \sigma_V^{\text{type}}(v_j)$.

(iv)–(vi) **Molecular case.** Element consistency gives a unique element type per class $[v]$. Shared-edge order consistency ensures any edge e appearing in overlaps has a unique bond order. Finally, valency balance enforces

$$\sum_{w: ([v], [w]) \in E'} \text{bo}([v], [w]) = R(v)$$

for each class $[v]$, where $R(v)$ is the total residual contributed by all local copies of that atom. Since residuals are defined as $\text{val}(v) -$ (intramolecular bond order already inside primitives), this equality guarantees that inter-token bonds exactly saturate the valence: neither deficits nor oversaturation can occur. \square

Corollary B.4 (Correctness by Construction). *If S' is obtained from a valid graph G via the decomposition of Section 3.1, then by Corollary B.2 there exists a satisfying assignment of ϕ_{hard} that reconstructs a graph G^* isomorphic to G . Conversely, by Theorem B.3, any satisfying assignment yields a valid G' ; in the molecular setting, G' also satisfies element consistency and valency exactly. Hence the hard constraints are sound (no invalid outputs) and complete for reassembling training graphs (every training graph has a satisfying witness).*

B.2. Constraints

Hard constraints (ϕ_{hard}): Below are the formal hard constraints we enforce:

(i) *Subgraph integrity.* Nodes from the same subgraph/token never merge. That is, $\forall u, v, m_{u,v} \implies u \in V_i, v \in V_j$ for some $i \neq j$

(ii) *Element consistency.* Merged atoms must have equal element types:

$$\forall u, v : m_{u,v} \implies \text{elem}(u) = \text{elem}(v).$$

(iii) *Valency cap.* Let the internal (within-primitive) bond-order degree of an atom $u \in V_i$ be

$$\text{deg}_i(u) = \sum_{(u,x) \in E_i} \text{bo}(u, x).$$

If two node-slot atoms $u \in V_i^{\text{slot}}$ and $v \in V_j^{\text{slot}}$ are merged via $m_{u,v}$, then the resulting atom cannot exceed the valency cap for its element:

$$m_{u,v} \Rightarrow \text{deg}_i(u) + \text{deg}_j(v) \leq \text{cap}(\text{elem}(u)).$$

(Here $\text{cap}(\cdot)$ is the allowed maximum valence for each element under the dataset’s chemistry conventions.)

(iv) *Edge-slot merges (fused/shared edges).* Edge sharing is only allowed for edges in E_i^{slot} and E_j^{slot} . Two edge-slot copies $e = (u, v) \in E_i^{\text{slot}}$ and $e' = (u', v') \in E_j^{\text{slot}}$, $i \neq j$ may be merged only if they (i) have the same bond order, and (ii) their endpoints are merged consistently:

$$\text{bo}(u, v) = \text{bo}(u', v') \wedge (m_{u,u'} \wedge m_{v,v'} \vee m_{u,v'} \wedge m_{v,u'}).$$

When such an edge merge occurs, we enforce endpoint element equality and valency caps *accounting for the duplicated edge*:

$$\begin{aligned} (m_{u,u'} \wedge m_{v,v'}) \Rightarrow \\ \text{elem}(u) = \text{elem}(u'), \\ \text{deg}_i(u) + \text{deg}_j(u') - \text{bo}(u, v) \leq \text{cap}(\text{elem}(u)), \\ \text{deg}_i(v) + \text{deg}_j(v') - \text{bo}(u, v) \leq \text{cap}(\text{elem}(v)). \end{aligned}$$

The swapped orientation $(m_{u,v'} \wedge m_{v,u'})$ uses the same constraints.

This subtraction of $\text{bo}(u, v)$ removes double-counting of the shared bond: it appears once in each primitive but becomes a single edge in G' .

(v) *Edge-slot restriction.* Edge merges are permitted only for edge-slot edges:

$$\begin{aligned} ((u, v) \notin E_i^{\text{slot}}) \vee ((u', v') \notin E_j^{\text{slot}}) \Rightarrow \\ \neg((m_{u,u'} \wedge m_{v,v'}) \vee (m_{u,v'} \wedge m_{v,u'})). \end{aligned}$$

In particular, an edge may be shared even if its endpoints are not node slots, provided the edge itself lies in E^{slot} .

B.3. The NSGGM algorithms and constraints

This appendix gives concise, implementation-ready pseudocode for training and inference.

Soft Constraints For Connectivity: Define $\text{par}[i]$ as the parent identified for subgraph token i in S' . Define

$\text{active}_i = \text{True}$ if the i th subgraph token is used in the final molecule, that is, any $m_{u,v} = \text{True}$ where $u \in V_i$. To encourage connectivity, we use hard constraints to define a valid reachability structure; actual connectivity is encouraged only via soft rewards.

Introduce Boolean reachability vars reach_i , root indicators isRoot_i , and integer distances dist_i . Add hard constraints: if any active_i then exactly one root; roots are active and have $\text{dist} = 0$. Add hard constraints: $\text{active}_i \Rightarrow \text{reach}_i$ and every reachable non-root i has a reachable parent j with $\text{conn}_{i,j}$ and $\text{dist}_i = \text{dist}_j + 1$. Add soft rewards to \mathcal{O} favoring larger connected assemblies:

$$\max \sum_i w_{\text{reach}}(i) \cdot \mathbf{1}[\text{reach}_i] + \sum_{i < j} w_{\text{conn}} \cdot \mathbf{1}[\text{conn}_{i,j}],$$

and if parents $\text{par}[i]$ are given, add an extra reward for $\text{conn}_{i,\text{par}[i]}$.

Algorithm 2 SMT-based assembly of a blueprint

Input: Blueprint $S' = \{P_i\}_{i=1}^k$; optional ϕ_{user}

Output: Selected merges $\{m_{u,v}\}$

```

16 Function ASSEMBLESMT( $S', \phi_{\text{user}}$ )
17    $\mathcal{O} \leftarrow \text{Z3OPTIMIZE}(); M \leftarrow \emptyset$  //  $M$  maps
      candidate pairs to Booleans  $m_{u,v}$ 
      // (1) Candidate merges + local validity
      clauses
18    $M \leftarrow \text{AddNodeMergeCandidates}(S', \mathcal{O})$ 
       $M \leftarrow M \cup \text{AddEdgeSlotCandidates}(S', \mathcal{O})$ 
      // Forced Merges/Structures/Rules from
      user
19   foreach user rule  $r \in \phi_{\text{user}}$  do
20     Identify the set of required atom pairs  $\mathcal{F}(r)$  induced by  $r$ 
       $\text{prefix}_r \Leftrightarrow \bigwedge_{(u,v) \in \mathcal{F}(r)} m_{u,v}$ 
21   if  $\phi_{\text{user}}$  provides logical constraints then
22      $\mathcal{O} \leftarrow \text{parseLogic}(\text{constraint}, \text{prefix}_i)$  // where
      parseLogic recursively parses
      the prefixes and  $S'$  required
      for logical constraints and adds
      corresponding clause for solver
      between them
23   foreach subgraph  $i \in \{1, \dots, k\}$  do
24     Define  $\text{active}_i \Leftrightarrow \bigvee \{m_{u,v} \in M : u \in P_i \text{ or } v \in P_i\}$ 
      // Connectivity (reachability) + soft
      objective defined in B.3
      // Solve and decode
25   Solve  $\mathcal{O}$  (Max-SMT) return return all true  $m_{u,v}$ 

```

Practical notes. (i) *Masking:* BuildFeasibilityMasks pre-computes per-position masks using only local interface checks (degree stubs, fused-cycle tuples), which is linear in the number of candidate tokens at each step. (ii) *User control:* ϕ_{user} may add hard clauses (e.g., ring-count bounds, forbidden motifs) or weighted soft terms that are optimized in the final SMT objective without retraining M_θ . (iii)

Caching: Since ϕ_{struct} depends only on \mathcal{V} , its encoding can be cached across runs.

B.4. Training

ELBO. We weight the contributions of the autoregressive token decoder and the three structural heads by $\lambda_{\text{tok}}, \lambda_{\pi}, \lambda_m, \lambda_{\text{meta}}$, and weight the KL regularizer by β .

$$\mathcal{L}_{\text{ELBO}} = \underbrace{\mathbb{E}_{z \sim q_{\phi}(z|\mathcal{G})}[\mathcal{R}_{\lambda}(z)]}_{\text{generator loss}} - \underbrace{\beta \text{KL}(q_{\phi} \| p_{\phi})}_{\text{latent alignment}}, \quad (9)$$

Here $\text{KL}(q_{\phi} \| p)$ denotes

$$\text{KL}(q_{\phi}(z | \mathcal{G}) \| p(z)), \quad \text{with } p(z) = \mathcal{N}(0, I).$$

, and the weighted reconstruction term is

$$\begin{aligned} \mathcal{R}_{\lambda}(z) = & \underbrace{\lambda_{\text{tok}} \mathcal{L}_{\text{tok}}(z)}_{\text{AR tokens}} \\ & + \underbrace{\lambda_{\pi} \mathcal{L}_{\pi}(z)}_{\text{parent pointers}} \\ & + \underbrace{\lambda_m \mathcal{L}_m(z)}_{\text{merge/interface}} \\ & + \underbrace{\lambda_{\text{meta}} \mathcal{L}_{\text{meta}}(z)}_{\text{metadata}}. \end{aligned} \quad (10)$$

The per-head log-likelihoods are

$$\mathcal{L}_{\{\text{tok}, \pi, m, \text{meta}\}}(z) = \sum_{\ell=1}^L \log p_{\theta}(x_{\ell} | c_{\ell}), \quad (11)$$

where

$$(x_{\ell}, c_{\ell}) \in \begin{cases} (g_{\ell}, (g_{<\ell}, z)), \\ (\pi_{\ell}, (\mathcal{T}, z)), \\ (m_{\ell}, (\mathcal{T}, z)), \\ (t_{\ell}, (\mathcal{T}, z)). \end{cases} \quad (12)$$

C. Dataset details

C.1. Molecular graph datasets

QM9 (Wu et al., 2018), MOSES and GuacaMol are molecular datasets, where nodes represent atoms and edges correspond to bonds. Planar dataset (Martinkus et al., 2022) is a non-molecular graph.

QM9. QM9 is a supervised, property-rich benchmark of small organic molecules (up to nine heavy atoms among {C,N,O,F}), each paired with a single low-energy 3D conformation and a suite of quantum-chemical targets (e.g.,

dipole moment, polarizability, energies). Its compact chemical space and dense labels make it ideal for studying message passing, geometry-aware encoders, and multi-task regression. QM9’s strength is label depth (node/edge/3D information and many targets), not breadth of chemotypes; it is less suitable for evaluating large-scale distribution learning.

MOSES. MOSES is a large, cleaned corpus for generative modeling drawn from drug-like ZINC subsets with standardized filters (e.g., MW, logP, allowed atom types). It ships with train/test splits and a unified metric suite (validity, uniqueness, FCD, KL, internal diversity), encouraging apples-to-apples comparison across unconditional generators. Unlike QM9, MOSES prioritizes scale and distributional realism over supervised labels; molecules are provided primarily as SMILES without per-atom/bond targets.

GuacaMol. GuacaMol is a broad, medicinal-chemistry benchmark that evaluates both distribution learning and goal-directed generation (e.g., multi-objective property optimization, rediscovery). It emphasizes realistic scaffold diversity and challenge tasks rather than supervised labels, providing standardized splits, metric implementations, and leaderboards. Practically, the dataset includes many chemically complex structures.

D. Experimental Details

D.1. Unconstrained Generation Details.

Hardware. Unconstrained generation experiments were ran on CPU-based compute only. Specifically, a *Google Colab CPU runtime* (Google Compute Engine VM) with an AMD EPYC 7B12 CPU (8 vCPUs) and 50 GB RAM, running Linux 6.6.105.

Throughput. Below (Table 6) we report the throughput on each benchmark, rounded to the nearest 10 molecules per second due to run-to-run variability.

Table 6. Inference throughput (mol/s) on the CPU runtime. Values are rounded to the nearest 10 mol/s.

Metric	QM9	GuacaMol	MOSES
Inference (mol/s)	20	40	100

D.2. Unconstrained Generation Examples.

D.3. Logical Constraints Satisfaction Specifications

Overview. We define formulations that evaluate global logical constraints over *substructure presence* in candidate molecules. Each instance is a propositional formula where each atom correspond to whether a molecule contains the corresponding scaffold. The tests contain: (i) set of drug-

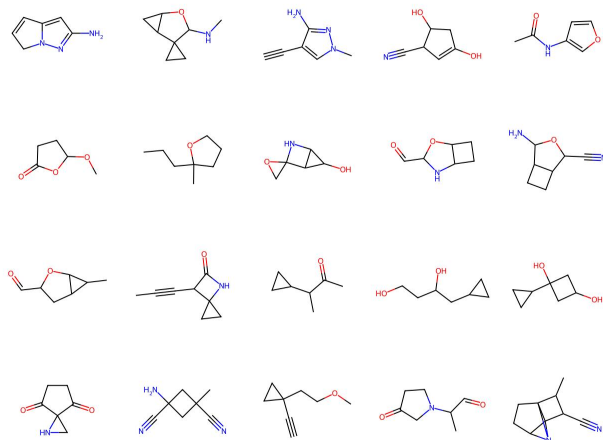


Figure 4. Example outputs from QM9 implicit. Samples were randomly chosen.

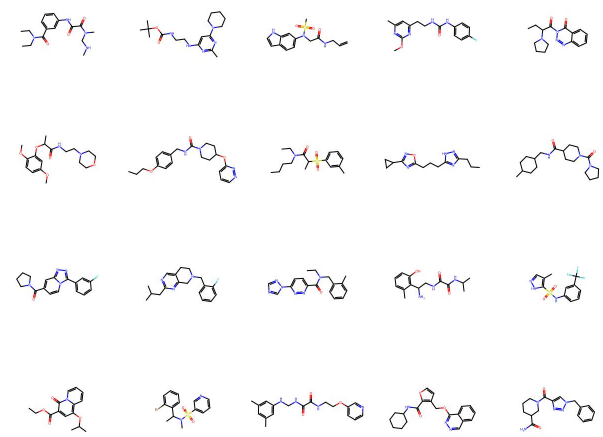


Figure 5. Example outputs from MOSES. Samples were randomly chosen.

like scaffolds (6–7 distinct pieces per formula) while remaining non-trivial, (ii) genuinely global/non-local logic via XOR parity, IFF statements, implications with composite antecedents, and conditional negations, (iii) ”sequential picking” behavior, where scaffold choice constrains compatible substituent families, and finally (iv) four instances: two moderately difficult satisfiable, higher-coverage constraints; one difficult and satisfiable but near-zero coverage on broad drug-like scaffolds; and one pure-logic UNSAT sanity check. **We emphasize that these logical expressions are not intended as medicinal-chemistry specifications or direct applicable drug-discovery constraints. These serve as controlled, synthetic, stress tests for evaluating our model.**

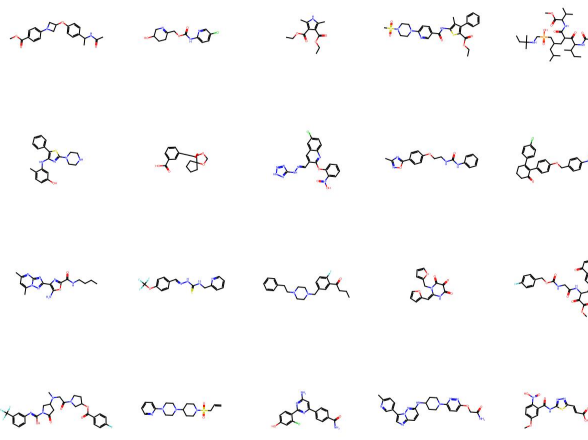


Figure 6. Example outputs from GuacaMol. Samples were randomly chosen.

Objects: pieces, atoms, and expression language. A *piece* is a named scaffold which can be composed by some *motifs*, g_1, \dots, g_n , where $g_i \in \mathcal{V}$. Let $S = \{s_1, \dots, s_n\}$ denote the set of pieces. Each piece s_i induces a Boolean atom x_i which is interpreted as “the output molecule, G' , contains s_i .” Formulas are built over these atoms using Boolean operators: negation \neg , conjunction \wedge , and disjunction \vee . No cardinality primitives are assumed; all “exactly-one” constraints are expressed compositionally (via XOR).

Core scaffolds. The core scaffolds are single-ring, non-fused heteroaromatics:

- **Pyridine:** (*PubChem CID 1049*)
- **Pyrimidine:** (*PubChem CID 9260*)
- **Imidazole:** (*PubChem CID 795*)
- **Thiazole:** (*PubChem CID 9256*)

Functional motifs (branches). The functional motifs are compact, generic patterns. Their corresponding SMILES string is noted below:

- **Nitrile:** C#N
- **Trifluoromethyl:** C(F)(F)F
- **Amide:** C(=O)N
- **Sulfonamide:** S(=O)(=O)N
- **Tert-Butyl group:** CC(C)(C)C

Logical operators macros. We define the following operators over Boolean expressions a, b :

$$\text{IMP}(a, b) := \neg a \vee b \quad (13)$$

$$\text{XOR2}(a, b) := (a \vee b) \wedge \neg(a \wedge b) \quad (14)$$

$$\text{IFF}(a, b) := \text{IMP}(a, b) \wedge \text{IMP}(b, a). \quad (15)$$

All benchmarks below are expressed using only \neg, \wedge, \vee plus these macros.

Assignment mapping and expression satisfaction.

Given a candidate molecule m and piece set S , we map m to a Boolean assignment $\alpha_m = (x_1(m), \dots, x_n(m))$ through its presence in the final molecule i.e.

$$x_i(m) = 1 \iff m \text{ contains the substructure query } s_i.$$

A molecule m satisfies a benchmark formula φ if $\varphi(\alpha_m) = \text{True}$. Then, we state $m \models \varphi$.

Expression 1 (φ_1):

Scaffolds used (7): Pyridine (P), Pyrimidine (Q), Nitrile (N), Trifluoromethyl (F), Amide (A), Sulfonamide (S), *Tert-Butyl* (T). We define three exactly-one selections:

$$\text{CORE12_X} := \text{XOR2}(P, Q), \quad (16)$$

$$\text{EWG_X} := \text{XOR2}(N, F), \quad (17)$$

$$\text{POL_X} := \text{XOR2}(A, S). \quad (18)$$

Full expression:

$$\begin{aligned} \varphi_1 := & \text{CORE12_X} \wedge \text{EWG_X} \wedge \text{POL_X} \\ & \wedge \text{IMP}(P, N \vee (F \wedge T)) \\ & \wedge \text{IMP}(Q, F \vee (N \wedge A)) \\ & \wedge \text{IMP}(T, S) \\ & \wedge \text{IMP}(A, \neg T). \end{aligned} \quad (19)$$

Intuitively, scaffold choice gates feasible EWG/polar modes, and bulk steers the polar choice which results in global coupling despite the small number of atoms.

Expression 2 (φ_2):

Scaffolds used (6): Imidazole (I), Thiazole (H), Nitrile (N), Amide (A), Sulfonamide (S), *tert-Butyl* (T). This expression enforces exactly-one core and exactly-one polar:

$$\text{CORE34_X} := \text{XOR2}(I, H), \quad (20)$$

$$\text{POL2_X} := \text{XOR2}(A, S). \quad (21)$$

Full expression:

$$\begin{aligned} \varphi_{B2} := & \text{CORE34_X} \wedge \text{POL2_X} \\ & \wedge \text{IFF}(T, S) \\ & \wedge \text{IMP}(A, N) \\ & \wedge \text{IMP}(H, A \wedge \neg T) \\ & \wedge \text{IMP}(I, S \vee N). \end{aligned} \quad (22)$$

This instance pushes on IFF wiring and implications with composite consequents.

Expression 3 (φ_3): Scaffolds used (7): Pyridine (P), Pyrimidine (Q), Thiazole (H), Nitrile (N), Trifluoromethyl (F), Amide (A), Sulfonamide (S). This expression requires the presence of three cores simultaneously, then select exactly one EWG and one polar, and finally lock consistent modes:

$$\begin{aligned} \varphi_{B3} := & (P \wedge Q \wedge H) \\ & \wedge \text{XOR2}(N, F) \wedge \text{XOR2}(A, S) \\ & \wedge \text{IFF}(A, N) \wedge \text{IFF}(S, F). \end{aligned} \quad (23)$$

Although it is logically satisfiable, the multi-core conjunction is intended to have a low hit rate in the training dataset.

Expression 4 (UNSAT) (φ_{UNSAT}):

Scaffolds used (3): Pyridine (P), Pyrimidine (Q), Imidazole (I). The expression is:

$$\varphi_{UNSAT} := \text{XOR2}(P, Q) \wedge \text{XOR2}(Q, I) \wedge \text{XOR2}(P, I). \quad (24)$$

This formula is unsatisfiable as pairwise XOR constraints among three variables cannot hold simultaneously. This serves as a sanity check of the logical layer.

Experiment chemistry constraints. Across all experiments, we apply a valency-only feasibility check. Bonds contribute their nominal order to the atom valence. Aromatic bonds are counted as 1.5. Default atomic valence limits follow common organic chemistry conventions (i.e., H = 1, C = 4, N = 3 / 5 with charge, ...). Formal charges adjust the allowed valence accordingly.

Transformer decoder sampler. For each dataset, we trained the sampler for 20 epochs using the Adam optimizer (learning rate 5×10^{-3} , batch size 128). The model is a lightweight GPT-style decoder with four layers, four attention heads, and 128 hidden dimensions. At inference time, we employed diverse beam search with nucleus sampling (top-p = 0.99) and top-k sampling (k = 1000). A global frequency of 1.0 is applied to discourage over-sampling frequent fragments.

E. LLM Usage

Large Language Models (LLMs) were used as a general-purpose assistive tool in the preparation of this work. Specifically, LLMs supported tasks such as refining the clarity of writing, suggesting alternative phrasings, and checking the consistency of technical terminology. They were **not** used for generating research ideas, conducting experiments, or

Table 7. Unconditional generation on SBM and planar graphs. V.U.N.: valid, unique & novel graphs.

Model	Deg ↓	Clus ↓	Orb ↓	V.U.N. ↑
<i>Stochastic block model</i>				
GraphRNN	6.9	1.7	3.1	5%
GRAN	14.1	1.7	2.1	25%
GG-GAN	4.4	2.1	2.3	25%
SPECTRE	1.9	1.6	1.6	53%
ConGress	34.1	3.1	4.5	0%
DiGress	1.6	1.5	1.7	74%
NSGGM (ours)	1.3	1.5	1.9	77%
<i>Planar graphs</i>				
GraphRNN	24.5	9.0	2508	0%
GRAN	3.5	1.4	1.8	0%
SPECTRE	2.5	2.5	2.4	25%
ConGress	23.8	8.8	2590	0%
DiGress	1.4	1.2	1.7	75%
NSGGM (ours)	1.3	1.1	2.0	72%

producing original scientific contributions. All substantive research decisions, analysis, and results presented in this paper are the responsibility of the authors. The authors have carefully reviewed and verified all LLM-assisted text to ensure accuracy and originality.

F. Non-Molecular Graph Dataset

The non-molecular benchmark of [Martinkus et al. \(2022\)](#) consists of two datasets of 200 graphs: (a) stochastic block models (SBM; up to 200 nodes) and (b) planar graphs (64 nodes). Following the protocol, we assess how well generated graphs match degree distributions (Deg), clustering coefficients (Clus), orbit counts (Orb), and the proportion of valid, unique, and novel graphs (V.U.N.).

NSGGM is used in an unconditional setting. The sampler proposes discrete construction sequences, which the symbolic solver assembles under task-specific constraints (e.g., simple connectivity for SBM and planarity for planar graphs). On *SBM*, NSGGM attains the lowest Deg error (1.3) and ties the best Clus (1.5), while remaining competitive on Orb (1.9), yielding the highest V.U.N. (77%). On *Planar*, NSGGM achieves the best Deg (1.3) and Clus (1.1) and competitive Orb (2.0), with V.U.N. 72%—close to DiGress (75%)—indicating strong fidelity to planar structure with minimal loss in novelty. These outcomes illustrate that explicit, verifiable constraints during assembly can improve structural metrics without sacrificing diversity.